RESEARCH ARTICLE

Flows on the nozzle plate of an inkjet printhead

**Bart Beulen · Jos de Jong · Hans Reinten ·
Marc van den Berg · Herman Wijshoff ·
Rini van Dongen**

Abstract Flow patterns of ink layers on the nozzle plate of a piezo-driven printhead are investigated. Two different flow types are identified. First, a jet of droplets induces a radial airflow in the direction of the jet, which in turn causes a liquid flow towards the nozzle. Second, the movement of the meniscus in the nozzle causes an equally strong flow, but completely different flow patterns. The results are presented in a phase diagram with pulse amplitude and firing frequency as parameters.

1 Introduction

Inkjet printing is being used in many applications besides printing on paper (Williams 2006). To ensure a stable and reproducible printing process, drop-on-demand (DOD) printing devices are often employed (Meacham et al. 2005; Chen and Basaran 2002; Yang et al. 1997).

B. Beulen (✉) · R. van Dongen
Department of Applied Physics,
Eindhoven University of Technology,
P.O. Box 513, 5600 MB Eindhoven, The Netherlands
e-mail: b.w.a.m.m.beulen@tue.nl

J. de Jong
Physics of Fluids group, Faculty of Science and Technology
and Burgers Center of Fluid Dynamics,
University of Twente, P.O. Box 217,
7500 AE Enschede, The Netherlands

H. Reinten · M. van den Berg · H. Wijshoff
Océ Technologies B.V., P.O. Box 101,
5900 MA Venlo, The Netherlands

In piezo-electric inkjet devices, a voltage pulse is applied to a piezo-electric element (Le 1998). This causes an ink-filled channel to deform, thereby creating a pressure waveform in the channel. Fluid acoustics are involved to guide the waveform energy towards the nozzle. Inside the nozzle a strong acceleration of fluid occurs, such that a droplet is generated (Bogy and Talke 1984).

This research focusses on a piezo-electric inkjet printhead with an array of ink channels. Each ink channel has its own piezo element which can be actuated independently. Typically, each nozzle has a firing frequency range up to 30 kHz. This firing frequency is called the DOD frequency. For the schematic setup of the printhead see Fig. 1.

The volume and velocity of the jetted droplets depend on the properties of the actuation pulse. For jetting, a 13 μs trapezoidal actuation pulse with an amplitude of 34 V is used to generate droplets with a volume of 30 pl and a velocity of 7 m/s. When decreasing the actuation amplitude, the droplet velocity decreases. At about 15 V the amplitude of the actuation pulse is too low to create droplets; only an oscillation of the meniscus in the nozzle occurs.

The droplets exit the printhead at the nozzle plate, which consists of a nickel plate with an array of nozzles in it. The nozzles have a spacing of 340 μm and a diameter of 30 μm or less. Figure 2 schematically shows a part of the nozzle plate. The circular areas around the nozzles are due to a difference in material structure, which is found to be irrelevant for this study.

For a successful printhead design, it is essential that the drop formation is a stable process. It is observed that after a period of jetting ($t \approx 5$ s), a thin ink layer
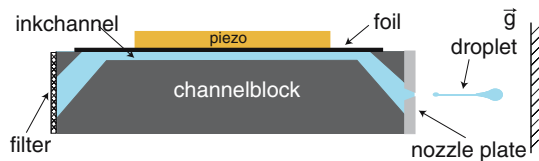
Fig. 1 Sketch of the geometry of the printhead. The ink channel (8 mm) is deformed by a moving piezo element, covered with a thin foil. Droplets are then ejected from the nozzle (30 μm in diameter). The jetted droplets have a typical volume of 30 pl

Fig. 3 Photograph of the ink layer on the nozzle plate. Interference patterns indicate a gradient in ink layer thickness. The thickness of the ink layer increases in the x direction

(10–30 μm) is formed on the nozzle plate. In general, the thickness of the ink layer increases in the x direction (Fig. 3). The presence of this ink layer can cause an increase of the probability of nozzle failure, as described by De Jong et al. (2006). Two failure mechanisms are identified (De jong et al. 2006), for both mechanisms, nozzle failure is caused by air entrapment. First, particles can reach the nozzle by transport in the ink layer. A particle near the nozzle can disturb the drop formation process upon which an air bubble can be formed that can cause nozzle failure. Secondly, upon actuation, ink from the nozzle plate can be pulled into the nozzle. At a critical ink layer thickness, an air filled cavity can be enclosed, which causes nozzle failure.

In this paper, we focus on the flow in the ink layer on the nozzle plate induced by the actuation of a single nozzle. First, a description of the ink layer is given in Sect. 2. The flow in the ink layer on the nozzle plate is then visualized by applying ink with tracer particles. Particle Tracking Velocimetry (PTV) is used to determine the flow fields (Sect. 3). Flow patterns when jetting are described in Sect. 4. Finally, in Sect. 5, the mechanisms responsible for the observed flows are discussed. In Sect. 6, a phase diagram with pulse amplitude and firing frequency as parameters is presented.
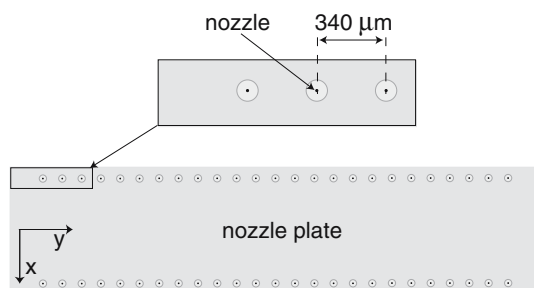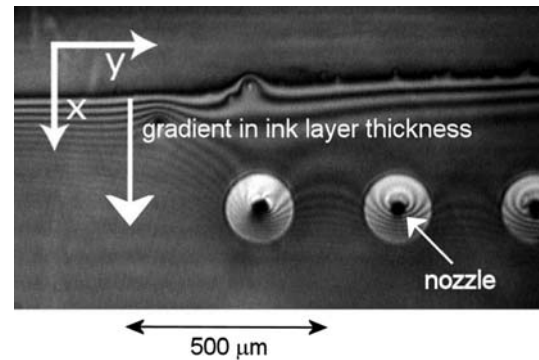
2 The ink layer

The wetting characteristics of the ink on the nozzle plate surface are functions of the surface energies of the nozzle plate–air interface, the ink–air interface and the nozzle plate–ink interface. Detailed knowledge of these energies and of the surfaces is not present. However, it is possible to quantify the wetting characteristics by determining the macroscopic contact angle of the ink on the nozzle plate surface. The contact angle, θ, is found to be less than 20°, which indicates that thin ink layers are formed. For excellent reviews on wetting phenomena and the dynamics of thin films, we refer the reader to De Gennes et al. (2004) and Oron et al. (1997).

Preliminary observations indicate that the ink layer can be described by a characteristic layer thickness $H = \mathcal{O}(10^{-5})$ m, a characteristic velocity of the ink, $V = \mathcal{O}(10^{-3})$ m/s and a characteristic radius of curvature $R = \mathcal{O}(10^{-3})$ m (Fig. 4).

The ink has a density, ρ, of $\mathcal{O}(10^3)$ kg/m³ a viscosity, μ, of $\mathcal{O}(10^{-2})$ kg/m/s and a surface tension, σ, of $\mathcal{O}(10^{-2})$ N/m. The Reynolds number of the flow in the ink layer, $Re_H = \rho V H/\mu$, is found to be $\mathcal{O}(10^{-3})$, which indicates that the flow is viscosity dominated. Assuming the shape of the ink layer can locally be described
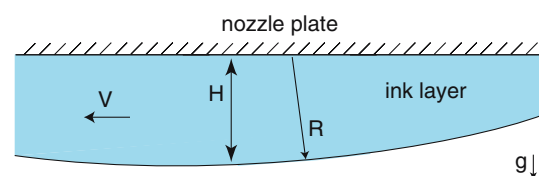

Fig. 2 Nozzle plate with two arrays of nozzles. The nozzles are spaced 340 μm, and have a diameter of 30 μm

Fig. 4 The ink layer present on the nozzle plate can locally be described by the parameters H, R and V

as a spherical cap, the gravity and capillary force can be estimated for $H << R$ as

$$F_{\text{gravity}} = \pi \rho g R H^2 \approx \mathcal{O}(10^{-9}) \, \text{N}, \quad (1)$$

$$F_{\text{capillary}} = 2\pi\sigma\sin\theta\sqrt{2RH} \approx \mathcal{O}(10^{-7}) \, \text{N}. \quad (2)$$

For this specific ink layer geometry, the gravity force is small compared to the capillary force (as expected from De Gennes 1985). The exact magnitudes of the gravity and capillary forces highly depend on the exact values of R and H, which are not known a priori. Moreover, the complete force description is very difficult to state because several driving mechanisms could play a role, as we will discuss in Sect. 5. This infers that an exact conclusion cannot yet be drawn.

3 Visualization

The nozzle plate is visualized using a 25-fps Watec LCL 902K video camera connected to an Olympus microscope. The camera axis is placed at 90° with respect to the printhead as shown in Fig. 5. To obtain a perpendicular image of the nozzle plate, a mirror is mounted at 45° just below the nozzle plate. An Olympus Highlight 3001 light source is used to illuminate the nozzle plate at normal incidence.

To prevent the jetted droplets from reaching the mirror, an air flow is applied between the printhead and the mirror. The air flow bends the droplets away from the mirror. To ensure that the air flow does not influence the movement of the ink layer on the nozzle plate, the air flow is applied using an injection needle. Figure 5 shows a schematic view of the experimental setup.

Particle Tracking Velocimetry is used to measure velocities of tracer particles in the ink layer. These tracer particles are melamine particles with a diameter of $2.00 \pm 0.06 \, \mu m$ and a density of $1.51 \times 10^3 \, \text{kg/m}^3$.
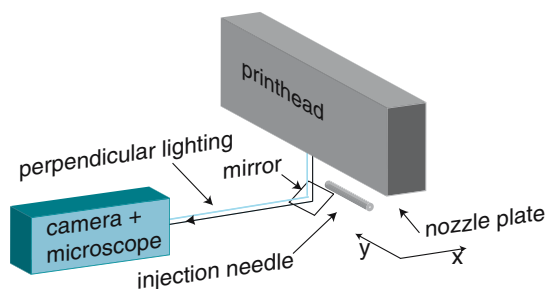
With a camera frame rate of 25 Hz, images are acquired every 0.04 s. To prevent motion blurring of the particles, the exposure time of the camera is set sufficiently short. The particles are identified by subtracting two subsequent images and applying an intensity threshold. The particles are then tracked over multiple frames and the trajectory is determined. The velocity is calculated from the positions of the particles and the interframe time.

The particles (of diameter $2 \, \mu m$) are displayed at approximately 9 pixels. The detection of the position of the particle has an accuracy of 1 pixel. The resolution of the images is $1.2 \, \mu m$ per pixel. To increase the accuracy, the velocity estimation is averaged over two frames. For the highest velocities of $1 \, \text{mm/s}$ this results in a relative error of 3%.

The ink with the particles is directly deposited on the nozzle plate near the nozzle of interest. After the ink reaches an equilibrium situation, actuation is started and the particle movement is recorded and analyzed.

4 Flow patterns when jetting

Experiments using a jetting nozzle are performed at DOD frequencies up to 30 kHz. In general, an unidirectional axial flow towards the nozzle occurs.

To get a better understanding of the unidirectional flow fields, the flow field at 25 kHz is determined. As described in the previous section, ink with particles is directly deposited on the nozzle plate. After an equilibrium is reached, actuation of a single nozzle is started. The movement of the particles is analyzed using PTV. The resulting particle lines are presented in Fig. 6.
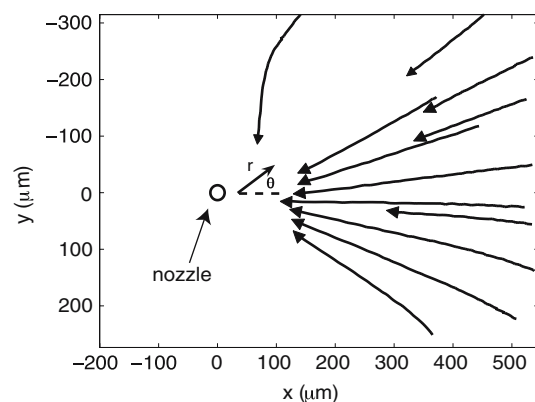
Fig. 6 Particle lines near a nozzle jetting at 25 kHz show a radial flow of ink towards this jetting nozzle. On the left side of the nozzle, no particles are tracked since no ink layer is present there

Fig. 5 Schematic view of the experimental setup

Since an ink layer is only present at the right side of the nozzle, particle lines can only be observed at the right side. The flow shows a radial symmetry of ink flowing towards the jetting nozzle. However, above and below the jetting nozzle, neighboring nozzles are disturbing the flow pattern. The ink flow cannot be tracked completely up to the nozzle, since its velocity becomes too high to be resolved with the camera. When the ink reaches the nozzle, it is presumably jetted away with the droplets.

By plotting the velocity of the particles as a function of the distance to the nozzle on a double logarithmic scale, the r dependency ($v \sim r^n$ with $|v| = \sqrt{v_\theta^2 + v_r^2}$) of the particle velocity is determined. This is done in Fig. 7 for multiple particle lines, where each color represents a different particle.

The slope is found to be $n = -1.3$, with a standard deviation of 0.3. For an ideal 2D sink flow, $n = -1$ is to be expected. The deviation is presumably caused by the gradient in the ink layer thickness.

When the nozzle is actuated with 20 kHz, a bi-directional radial flow occurs, as shown in Fig. 8.

The radial velocity, v_r, and the circumferential velocity, v_θ, of the tracked particles are presented in Fig. 9. The radial properties of the flow are confirmed by $v_\theta \ll v_r$.

The v_r velocity component indicates that one part of the particles is traveling towards the nozzle ($v_r > 0$) while another part of the particles is traveling away from the nozzle ($v_r < 0$). The video sequence shows that the two different directions of particle motion occur at the same position and the same time on the nozzle plate, indicating a depth-dependent velocity in the ink layer.
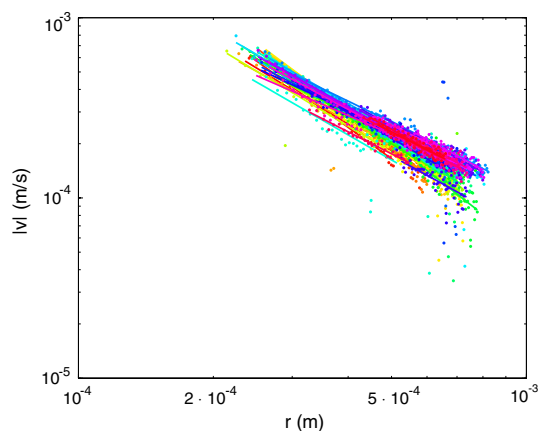
The depth dependency of the velocity profile is determined by placing a camera at 45° with respect to the nozzle plate. Because light reflects on the nozzle plate, the position of the particles in depth can be determined by using the mirror images of the particles. This experiment shows that the ink at the ink–air interface is moving towards the nozzle while the ink closest to the nozzle plate moves away from the nozzle. The resulting velocity profile, a Couette velocity profile, is depicted in Fig. 10.

The bi-directional flow at 20 kHz indicates that, except surface tension, other mechanisms are responsible for the ink flow on the nozzle plate. These mechanisms are identified and discussed in the next section.

5 Origin of the flows

As mentioned in Sect. 3, the flow of ink on the nozzle plate can easily be influenced by an air flow. Furthermore, vibrations such as the movement of the meniscus in the nozzle and the vibration of the entire nozzle plate due to the actuation of the piezos might cause an ink flow.

Experiments using a Speckle interferometer indicate that the amplitude of the vibration of the nozzle plate is $\mathcal{O}(10^{-9})$ m, which is negligible compared to the amplitude of the oscillation of the meniscus in the nozzle ($\mathcal{O}(10^{-5})$ m). This makes it more likely that the observed flows are caused by the meniscus motion. In this section, the influence of the induced air flow and the meniscus motion on the ink flow on the nozzle plate is determined.
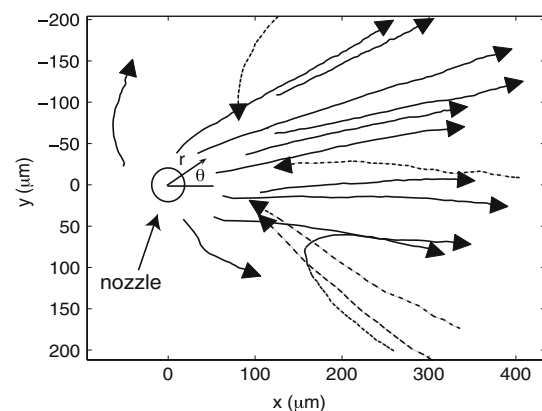

Fig. 7 Velocity of the particles as a function of the distance to a nozzle jetting at 25 kHz. Each color represents a different particle trajectory. The fits indicate a $v \sim r^n$ dependency of the flow in the ink layer on the nozzle plate with $n = -1.3$ with a standard deviation of 0.3

Fig. 8 Particle lines of the flow near a nozzle jetting at 20 kHz show particles moving towards the nozzle (*dashed lines*) and particles moving away from the nozzle (*continuous lines*), indicating a depth-dependent velocity in the ink layer

Fig. 9 Velocity components of the flow near a nozzle jetting at 20 kHz. Each color represents a different particle trajectory. The v_r component indicates that one part of the particles is moving towards the nozzle while another part is moving from the nozzle. The radial flow properties are confirmed since $v_\theta \ll v_r$
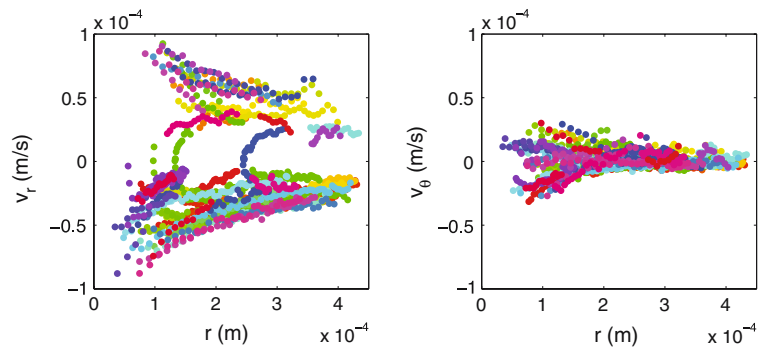
5.1 Air flow

A jet of droplets moving through air transfers momentum to the surrounding air (Lee 1976; Schlichting 1979). This causes an acceleration of the surrounding air and subsequently a suction of air towards the jet of droplets. First, the presence of the air flow is visualized by smoke injected in the air close to the jetting nozzle. Figure 11 shows a streamline of the air flow induced by the jetted droplets.

To be more quantitative, the momentum transfer to the surrounding air is shown with the high-speed Phantom V7 camera at a frame rate of 10 kfps. Figure 12 shows ten consecutive frames of the recording of the high-speed camera. Each frame shows two successive jetted droplets (in vertical direction).

Two droplets pass the jet in horizontal direction and are influenced by the air flow induced by vertically jetted droplets. Due to the limited depth of field (about 20 μm), it can be determined that one of the droplets is moving closer to the jet. It is apparent that the droplet moving the closest to the jet is influenced the most by the air flow.

Further analysis of the high-speed recording indicates that the horizontal moving droplets experience an average vertical acceleration of about 1,000 m/s².
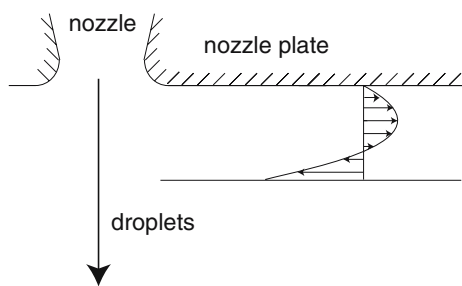
The average air flow velocity experienced by the horizontal moving droplets is determined by Stokes' law,

$$F_D = 6\pi\mu_a v_a R_d = m_d a_d, \qquad (3)$$

where μ_a is the viscosity of air, v_a is the relative velocity, R_d is the radius of the droplet, m_d the mass of the droplet and a_d the average acceleration experienced by the droplet. Assuming spherical droplets with a volume of 30 pl and a viscosity of air of 2×10^{-5} kg/m/s, the average experienced air flow velocity is determined to be about 4 m/s (about 60% of the jetted droplet velocity).

In a third experiment the geometry of the nozzle plate is modified to decouple the ink layer on the nozzle plate from the meniscus motion. On the modified nozzle plate, the jetting nozzle is surrounded by a
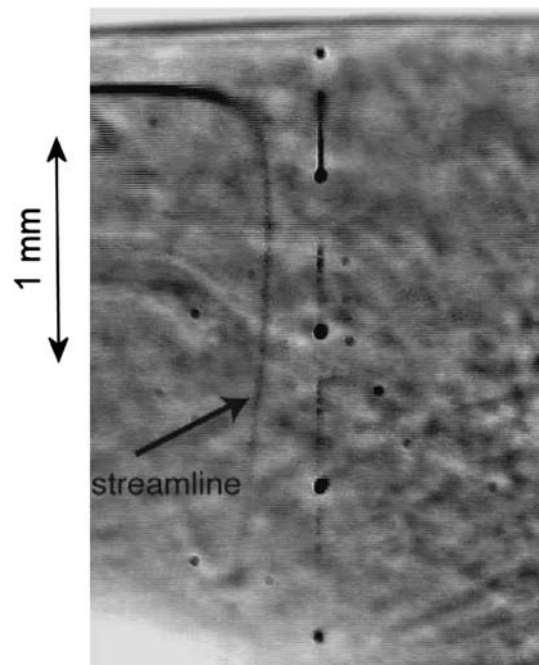
Fig. 10 The velocity profile at 20 kHz near the nozzle. The ink closest to the nozzle plate moves away from the jetting nozzle, while the ink closes to the ink–air surface is moved towards the jetting nozzle

Fig. 11 A streamline, visualized by the smoke, indicates the air flow near the jet of droplets
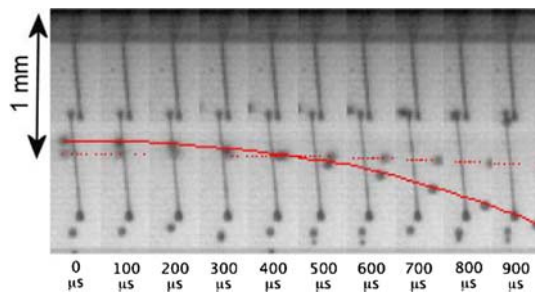
Fig. 12 Ten consecutive frames of the high-speed camera show ten droplets being jetted while two droplets pass the jet in horizontal direction. The air flow induced by the jet causes a momentum transfer to the horizontal moving droplets. Using the limited depth of field of the camera, it is determined that a droplet moving close to the jet (*continuous line*) is bent more than a droplet moving far from the jet (*dashed line*)

circular area with a radius of about 500 μm and a depth of 50 μm, as shown in Fig. 13. As the contact line of the ink is pinned to the edge of the circular area, fluid interaction between the local wetting and the global wetting is prevented.

Ink with particles is applied outside the circular area around the nozzle. When the ink reaches an equilibrium, jetting is started at 25 kHz. The resulting particle lines are presented in Fig. 14.

The particle lines show a flow towards the nozzle. Analysis shows that the flow velocity at $r = 500$ μm is $\mathcal{O}(10^{-5})$ m/s, which is comparable to the velocity observed at equal distance from the nozzle when jetting with the standard nozzle plate. Since the modified nozzle plate geometry prevents fluid interaction between the global and the local wetting, the movement of the global wetting can only be influenced by the presence of an air flow. Close to the edge of the circular area, however, deviations from the sink flow character occur due to the accumulation of ink.

The experiments indicate that the jetted droplets induce an air flow which is subsequently strong enough to influence the movement of the ink layer.
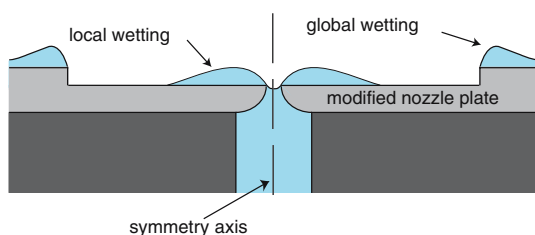

Fig. 13 Schematic view of the modified nozzle plate geometry, showing the local and the global wetting
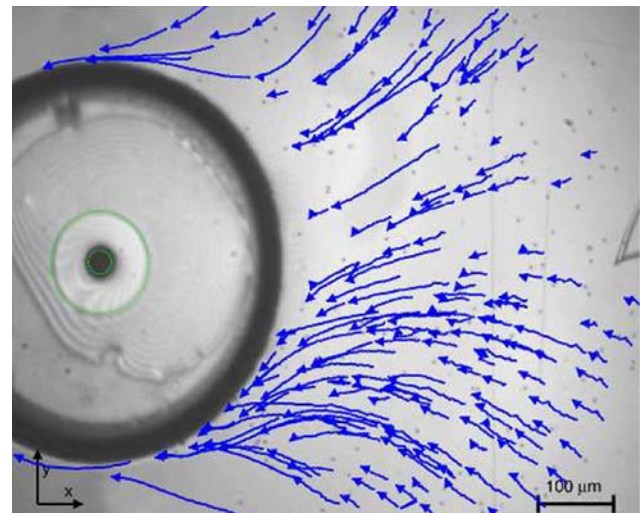

Fig. 14 The jet of droplets (25 kHz) induces a movement of ink towards the nozzle without ink contact between the meniscus and the ink layer

5.2 Meniscus motion

To check if the meniscus motion is capable of causing flow on the nozzle plate, experiments are performed using non-jetting actuation. When no droplets are jetted, the air flow is removed and the influence of the meniscus motion can be studied.

For very low actuation voltages, the nozzle shows no activity. Upon increasing the actuation voltage, the nozzle starts acting as a source of ink. The necessary actuation amplitude for the non-jetting actuation is determined by lowering the actuation voltage of a jetting nozzle until the jetting stops. This assures that the meniscus motion is at its maximum. For 20 kHz, this transition occurs at an actuation amplitude of 15 ± 1 V.

An experiment using non-jetting actuation is performed at 20 kHz and the resulting particle lines are presented in Fig. 15. The particle lines resemble the streamlines of a dipole, with the direction of the dipole along the gradient in the ink layer thickness.

The character of the r dependency is again determined by plotting the velocity as a function of the distance to the nozzle, on a double logarithmic scale (Fig. 16).

It is determined that $n = -2.3$ with a standard deviation of 0.3. An ideal 2D dipole flow would yield $n = -2$. The deviation is caused by the gradient in the ink layer thickness.

The experiment indicates that non-jetting actuation can cause equally strong flows on the nozzle plate as in the jetting actuation. However, the flow pattern is totally different.
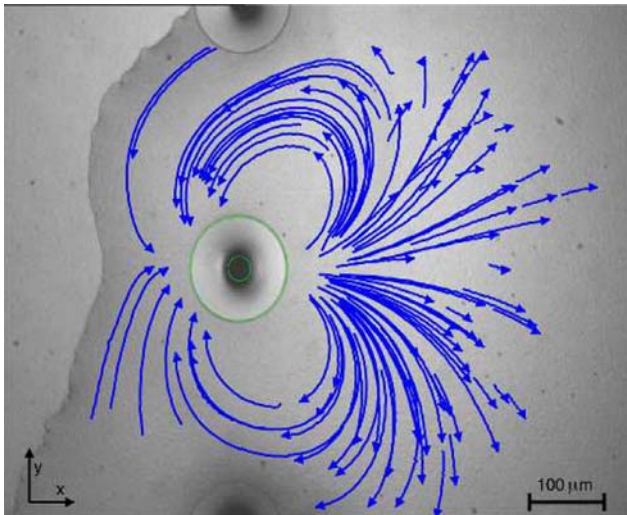
Fig. 15 Particle lines of the flow near a nozzle using non-jetting actuation at 20 kHz/15 V indicate a dipole flow

Fig. 16 Velocity of the particles as a function of the distance from the nozzle which is actuated using a non-jetting actuation at 20 kHz. Each color represents a different particle trajectory. The fits indicate a $v \sim r^n$ dependency of the flow in the ink layer on the nozzle plate with $n = -2.3$ with a standard deviation of 0.3

One possible mechanism of the net flow caused by the vibrating meniscus in the nozzle is acoustic streaming (Lighthill 1978; Squires and Quake 2005; Marmottant and Hilgenfeldt 2003). Acoustic streaming is directly related to the damping of acoustic waves, which implies that the time average momentum in an acoustic beam is transferred to an increase of time average pressure. In this particular case, the waves are capillary waves that are generated by the vibrating meniscus. Again, damping of these waves will lead to an increase of time average pressure or decrease of layer thickness, which in turn may lead to secondary flow. The details of such a flow field will depend on the details of the emitted capillary wave pattern and, therefore, also on the global time average spatial distribution of the layer thickness.

A second possible mechanism is a surface tension gradient-driven flow or Marangoni flow. The ink used consists of multiple components. It is known that by exposing such a liquid to a surface vibration, local changes in surface tension can occur (Wasan et al. 2001). If so, gradients in surface tension are to be expected, leading to Marangoni flows.

6 Phase diagram

As already mentioned in the previous section, the nozzle shows no activity at low actuation voltages. At intermediate actuation voltages the nozzle starts acting as a source of ink. Further increasing the actuation voltage causes a dipole flow just below the transition voltage from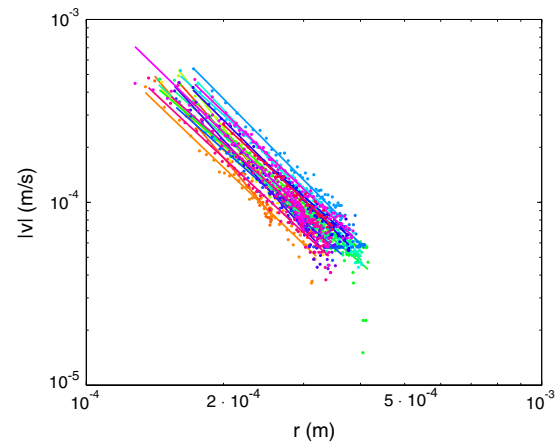 non-jetting to jetting. The various transitions that occur in the flow fields near the nozzle are determined for actuation amplitudes from zero to jetting amplitude and for jetting frequencies varying from 1 to 30 kHz. An overview of the states of the nozzle is presented in Fig. 17.

For frequencies above 19 kHz, there is a small region in (f,V)-space in which a non-jetting nozzle acts as a sink.

7 Conclusions and discussion

Actuation of a single nozzle with a sufficiently high voltage can induce a flow in the ink layer on the nozzle plate. Several flow patterns, depending on the actua-
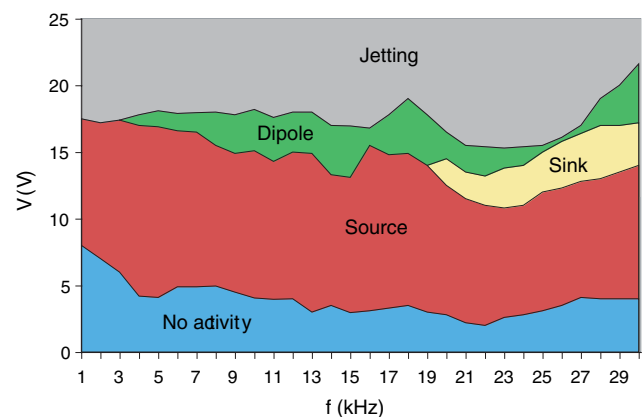

Fig. 17 Phase diagram of the nozzle, showing the different nozzle states as a function of the actuation amplitude and firing frequency

tion amplitude and frequency, are observed on the nozzle plate.

In the case of jetting actuation, the jet of droplets transfers momentum to the surrounding air, which results in a suction of air towards the jet. Friction between the ink layer and the air flow induced by the jet of droplets causes a radial flow of ink towards the nozzle. The flow resembles an ideal 2D sink flow, but a small deviation occurs due to the non-uniform ink layer thickness.

In the case of non-jetting actuation, the motion of the meniscus in the nozzle is strong enough to cause an equally strong ink flow on the nozzle plate. The most striking is the dipole-like flow, with the direction of the dipole always aligned along the ink layer thickness gradient. Small deviations from an ideal 2D dipole occur due to a non-uniform ink layer thickness. Two possible driving mechanisms for the flow induced by the meniscus motion are

1. Acoustic streaming due to capillary waves
2. Marangoni flow caused by local changes in surface tension.

The majority of the experiments shows a flow in the ink layer towards the actuated nozzle. Particles caught in this ink layer are likely to reach the jetting nozzle and may cause nozzle failure. For increasing the jetting stability of the printhead, an ink layer near the nozzles should be prevented. The absence of the ink layer would prevent transport of particles towards the nozzle. This can be achieved by using a nozzle plate with poor wetting properties, or by creating specific structures on the nozzle plate to prevent the formation of an ink layer.

References

Bogy DB, Talke FE (1984) Experimental and theoretical study of wave propagation phenomena in drop-on-demand inkjet devices. IBM J Res Dev 28(3):314–320

Chen A, Basaran O (2002) A new method for significantly reducing drop radius without reducing nozzle radius in drop-on-demand drop production. Phys Fluids 14(L1)

De Gennes PG (1985) Wetting: statics and dynamics. Rev Mod Phys 57(3):827–863

De Gennes PG, Brochard-Wyart F, Quere D (2004) Capillarity and wetting phenomena, drops, bubbles, pearls, waves. Springer, Berlin Heidelberg New York

De Jong J, Reinten H, Van den Berg M, Wijshoff H, Versluis M, De Bruin G, Lohse D (2006) Air entrapment in piezo-driven inkjet printheads. J Acoust Soc Am 120(3):1257–1265

Le HP (1998) Progress and trends in ink-jet printing technology. J Imaging Sci Technol 42(1):49

Lee HC (1976) Boundary layer around liquid jet. IBM J Res Dev 21(1):48–51

Lighthill MJ (1978) Waves in fluids. Cambridge University Press, Cambridge

Marmottant P, Hilgenfeldt S (2003) Controlled vesicle deformation and lysis by single oscillating bubbles. Nature 423:153–156

Meacham JM, Varady MJ, Degertekin FL, Fedorov AG (2005) Droplet formation and ejection from a micromachined ultrasonic droplet generator: visualization and scaling. Phys Fluids 17(100605)

Oron A, Davis SH, George Bankoff S (1997) Long-scale evolution of thin liquid films. Rev Mod Phys 69(3):931–980

Schlichting H (1979) Boundary layer theory. McGraw-Hill, New York, pp 230–235

Squires T, Quake S (2005) Microfluidics: fluid physics at nanoliter scale. Rev Mod Phys 77(3):977–1026

Wasan DT, Nikolov AD, Brenner H (2001) Droplets speeding on surfaces. Science 291(5504):605–606

Williams C (2006) Ink-jet printers go beyond paper. Phys World 19(24)

Yang JC, Chien W, King M, Grosshandler WL (1997) A simple piezoelectric droplet generator. Exp Fluids 23:445–447